Electric-field-induced structuring and rheological properties of kaolinite and halloysite

Zbigniew Rozynek[a], Tomáš Zacher[b], Marián Janek[b], Mária Čaplovičová[c] and Jon Otto Fossum[a,d]

[a] Department of Physics, NTNU, Høgskoleringen 5, NO-7491 Trondheim, Norway
[b] Department of Physical and Theoretical Chemistry, Faculty of Natural Sciences, Comenius University, Mlynská dolina CH1, SK-84215 Bratislava, Slovakia
[c] Department of Geology of Mineral Deposits, Faculty of Natural Sciences, Comenius University, Mlynská dolina CH2, SK-84215 Bratislava, Slovakia
[d] Centre for Advanced Study at the Norwegian Academy of Science and Letters, Drammensvegen 78, 0271 Oslo, Norway

Abstract

Electric-field-induced structuring of kaolinite and halloysite particles was studied in respect to their electrorheological (ER) response in silicone oil and in paraffin dispersions. The structural and morphological properties of both clay minerals were studied by XRD, FTIR, SEM, TEM and TGA techniques. The dipolar arrangement induced under application of an electric field was investigated by 2D-WAXS and optical microscopy techniques. The ER response of the samples was measured by both the shear rate controlled method and bifurcation tests. Kaolinite particle dispersions were found to have an improved ER response relative to dispersions of halloysite particles. Finally, the electric currents of these ER fluids were measured and the results revealed differences in the current-magnitude between halloysite- and kaolinite-based silicone oil dispersions.

Keywords: kaolinite, halloysite, XRD, FTIR, electron microscopy, rheology

e-mail: zbigniew.rozynek@ntnu.no and janek@fns.uniba.sk

1. Introduction

Both kaolinite and halloysite belong to the kaolinite group of minerals having essentially similar chemical composition with the nominal formula $Al_2Si_2O_5(OH)_4$ per half unit cell, and they have important structural layer stacking differences. Natural kaolinites have various degree of structural disorder or "crystallinity", which is often related to the conditions of genesis of the particular mineral (Brindley et al., 1986; Giese, 1988; Madejová et al., 1997). Therefore, kaolinites are classified as either low defect or high defect kaolinites depending on their varying degrees of order in the crystal structure (Brindley et al., 1947). Halloysite differs intrinsically from the kaolinite in its layer stacking sequence. It can intercalate a monolayer of water molecules between the aluminosilicate layers and therefore the existence of two different mineral species of halloysite have been reported, namely the anhydrous 7 Å form and its hydrated 10 Å form, marked also as *halloysite* (*7Å*) and *halloysite* (*10Å*), respectively. The stoichiometry of halloysite (10Å) follows approximately the formula $Al_2Si_2O_5(OH)_4 \cdot 2H_2O$ per half unit cell. This hydrated form converts easily into the dehydrated form at atmospheric pressure, when dried at temperatures above 60°C, or in vacuum at room temperature. The anhydrous form with a basal spacing near 7.2 Å is metastable, and can recover its interlayer water in a wet environment. Particles of halloysite consist of tubes, rolls and cylinders, as well as irregular or spheroidal particles, whereas disc-like shapes are mainly expected for kaolinite particles. Halloysite presents a highly disordered structure, with random dislocations and shifts in both the *a* and *b* crystallographic directions (Brindley et al., 1946). The reason for the curvature of the layers is usually attributed to the lateral misfit between the octahedral and tetrahedral sheets in the structure of halloysite (Bates et al., 1959). It was postulated that stacking disorder plays an important role for hydration of kaolinite and formation of halloysite (Costanzo et al., 1984~~; Costanzo et al., 1984~~a, b). Because the 1:1

layers in hydrated halloysite are separated from each other by a layer of water molecules, and due to higher structural disorder, halloysite have usually a larger cation exchange capacity and surface area than kaolinite (Costanzo et al., 1985; Gardolinski et al., 2003; Nicolini et al., 2009; Cheng et al., 2010).

With respect to the chemical identity but different morphology of kaolinite and halloysite particles, the effect of an electric field on electrorheological (ER) properties of silicone oil dispersions of both clay minerals have been investigated. Such investigations are important for practical utilisations of ER fluids in future mechanical coupler and/or junction devices, or in designing electrical birefringent devices. Most of the previously studied clay mineral dispersions were water-based systems. (e.g. Chassagne at al., (2009) reported the electrophoretic mobility of kaolinite dispersions for different types of salt, various pH and ionic strengths; Rowlands et al. (1995) investigated the dynamic mobility and dielectric response of kaolinite particles; rheological properties of aqueous kaolinite dispersions were investigated by Lagaly (1989). However, to our knowledge, there are no data published yet for halloysite particles concerning electrokinetic response in non-polar media, and in particular not much information can be found regarding the comparison of ER behaviours of kaolinite and halloysite particles in respect to their different morphologies.

2. Samples and experimental techniques

2.1. Sample preparation

Kaolin from a primary deposit in Bayern-Oberpfalz was used in this study. The purified sample received from Hirschau, Germany, was washed with distilled water (conductivity ~1.0 µS), dried at 65°C, and crushed in an agate mortar before the characterization measurements (referred as Kaol). The halloysite sample was from a primary deposit located at Michalovce -

Biela Hora. Soluble phases of iron oxide/-hydroxides were removed according to the procedure of Tributh et al. (1986a, b). This procedure includes removal of carbonates, iron oxohydroxides, organic matter such as humic material and size fractionation. The fine fraction of halloysite particles was prepared by a sedimentation method using Stoke´s equation. Collected fine particles were centrifuged, washed with distilled water (conductivity ~1.0 µS), dried at 65°C, and crushed in an agate mortar before performing the characterization measurements (referred as Hal).

For rheological measurements dispersions of Kaol and Hal in silicone oil (~5 m%) were prepared by mixing in an orbital shaker for minimum 12 hours and applying 30 minutes of ultrasonication prior to each rheological and current measurement.

Kaol/paraffin and Hal/paraffin composites were prepared (instead of silicone oil-based dispersions) for wide-angle X-ray scattering (WAXS) experiments, since the position of a diffuse Bragg diffraction peak from silicone oil overlaps with the 001 Bragg reflection from both clay minerals. The composites were prepared as following: 1.4 g of each clay mineral powder was slowly added into 7g of already pre-melted paraffin-wax (120-130°C). After vigorous stirring, the dispersions were left undisturbed for 5 minutes to let the largest aggregates sediment and then the top portion (80 %) was poured into a new 10 ml glass vial. The dispersions were kept at ~125°C under stirring. After 2 hours four samples were prepared and these included: Kaol/paraffin and Hal/paraffin composites cast with and without *E*-field present. After the samples solidified, having a form of stripes (~15 x 6.5 x 1.5 mm), the WAXS measurements were performed. Optical microscopy measurements were done using low concentration (below 0.5 m%) clay mineral in oil dispersions (for observation clarity).

2.2. Experimental techniques

2.2.1. XRD

X-ray diffraction (XRD) patterns from kaolinite and halloysite powders were obtained using a PHILIPS PW 1710 X-ray powder diffractometer equipped with a Graphite monochromator PW 1752 and Cu radiation ($CuK\alpha_1$ λ=0.154056 nm). The patterns were scanned in the range of 4-70° in 2θ with a step size of 0.02° and a counting time of 2.0 s/step.

2.2.2. FTIR

Infrared spectra of the Kaol and Hal samples were obtained using a Nicolet 6700 Fourier Transform Infrared (FTIR) spectrometer from Thermo Scientific. The KBr pressed disk technique (0.5 mg of sample and 200 mg KBr) was used to get spectra in the MIR region (4000–400cm^{-1}). The discs were heated in a furnace overnight at 130°C to minimize the water adsorbed on KBr and the clay mineral sample. For each sample 128 scans with the resolution of 4 cm^{-1} were recorded. Spectra manipulations were performed using the Thermo Scientific OMNIC^{TM} software package.

2.2.3. TGA~~/DTG~~

Thermal gravimetric analysis (TGA) was performed on a TGA/SDTA851^{e} instrument (Mettler Toledo As.) with a heating rate of 2ºC/min up to 800°C under static air conditions. About 20 mg of sample was supplied to the Alumina crucible (with no lid covered).

2.2.4. TEM/SEM

Transmission electron microscopy (TEM) images of Kaol and Hal were recorded on a JEOL JEM-2000FX transmission electron microscope with an accelerating voltage of 160 kV. For this characterization the samples were prepared as follows: Kaol and Hal ethanol dispersions were treated 5 minutes by ultrasounds. Then a drop of the sample was spilled on a copper reticle coated colloidal film with a layer of carbon and finally the sample was dried at room temperature.

Scanning electron micrographs (SEM) were acquired using a field emission scanning electron microscope (Zeiss Ultra, 55 Limited Edition, accelerated voltage 10-15kV). For the

SEM samples, a dispersion of a small amount (<0.01 m%) of sample was dispersed in de-ionized water and ultrasonicated for 1 hour, and then pipetted onto a SEM stub. Before images were collected, all samples were carbon-coated in a conventional coating unit.

2.2.5. WAXS

The WAXS experiment was carried out at the European Synchrotron Radiation Facility (ESRF) in Grenoble, France. An X-ray beam with a wavelength of 0.9 Å and a 0.5 × 0.5 mm^2 beam size at the sample was used. The Swiss-Norwegian beamline (SNBL) BM01A is equipped with a two-dimensional MAR345 image plate detector with a diameter of 345 mm. The sample to detector distance was set to 350 mm, enabling the detection of scattering in a *q*-range of approximately 0.65 – 17 nm^{-1}, which corresponds to the real space *d*-range of 0.37 – 10 nm.

2.2.6. Rheometry and current measurements

The rheological properties of the clay mineral dispersions were measured under direct current (DC) electric fields using a Physica MCR300 Rotational Rheometer equipped with a coaxial cylinder (Physica ERD CC/27). All the rheological measurements were performed at constant temperature of 23°C. These included controlled shear rate tests for measuring shear stress as a function of shear rate and bifurcation measurements. In the former experiment the so-called flow curves were collected in the shear rate range between 0.1 and 1000 s^{-1} and fitted to Herschel–Bulkley model in order to obtain the static yield stresses for samples at different *E*-field strengths, namely 250, 500, 750, 1000, 1500 and 2000 V/mm, respectively. The bifurcation tests were performed as a complementary method to verify the values of the yield stresses. In this method samples were forced to flow under a constant stress, and then let to evolve in the presence of an *E*-field (see details in section 3.7). In addition, current

measurements were performed (in the same rheological cell) using an Agilent 34401A multimeter.

3. Results and discussion

3.1. XRD analysis

The structural and morphological properties of layered clay minerals can be indirectly deduced from their diffraction patterns. XRD patterns of both samples are shown in Figure 1A. The transition from the sharp diffraction peaks in Kaol to the mainly diffuse and "tailed" reflections in the pattern of Hal are shown, indicating decreased layer stacking order of the Hal sample. The *d*-spacing of the first basal reflections are 0.71 nm and 0.74 nm, for Kaol and Hal respectively. We suppose that an almost anhydrous form of halloysite was used in the experiments ~~(see TGA/DTG analysis in section 3.3)~~. The group of reflections from 020 to 002 particularly reflects the change of structural disorder. In this region the clearly resolved doublet $11\bar{1}$ and $1\bar{1}\bar{1}$ of the Kaol sample yields a single broadened reflection for the Hal sample (Figure 1B). This represents evidence for the increase in structural disorder for Hal (Grim, 1968).

3.2. FTIR spectroscopy.

FTIR was used as a complementary method to the XRD to investigate possible mineral admixtures in the samples. ~~IR spectra serve as a fingerprint pattern for mineral identification and gives unique information about the mineral structure (Madejová et al., 2001).~~ Well-ordered Kaol samples revealed four clearly-resolved absorption bands in the OH stretching region 3693-3620 cm^{-1} (Figure 2). A strong band at 3696 cm^{-1} is related to the in-phase symmetric stretching vibration, two weak absorptions at 3668 and 3652 cm^{-1} are assigned to out-of-plane stretching vibrations (Farmer, 2000; Madejová et al., 2002). In contrary, the IR

spectrum of Hal shows intensive absorption bands only at 3696 and 3621 cm^{-1} in the OH stretching region. The very low intensity of OH stretching bands at 3671 and 3652 cm^{-1} reflect a poorly ordered structure typical for halloysite samples (Brindley et al., 1947).

Structural stretching and bending as well as OH bending absorption bands are in the region 1300–400 cm^{-1} (Figure 2). Differences in layer stacking arrangement of the basic layers are reflected in the positions and shape of the bands. Clear differences between Kaol and Hal can be seen in the 1300-400 cm^{-1} region. The AlAlOH bending bands at 937 and 912 cm^{-1} for Kaol are detected as a shoulder near 939 cm^{-1} and as a distinct band at 913 cm^{-1} for Hal. The band at 430 cm^{-1} was observed in both Kaol and Hal spectra and belongs to Si-O deformation vibrations (Madejová et al., 2002). The inset in Figure 2 shows the details of OH stretching bands located at 3654 and 3649 cm^{-1}. These are typical wavelengths for OH vibrations from kaolinite, thus a small fraction of kaolinite-like particles is expected to be present in the Hal sample.~~The insert in Figure 2 (region 3700-3600 cm^{-1}) shows also stretching bands typical for kaolinite in the Hal sample at 3654 and 3649 cm^{-1}, indicating that kaolinite-like particles are present in the halloysite.~~ However, no other mineral admixtures or impurities were detected by the FTIR technique.

3.3. TGA/DTG

TGA was conducted mainly to prove the mineral purity and water content in both minerals. Figure 3 shows typical TGA/DTG behaviour of both the Kaol and the Hal samples in the temperature window 50-800°C.

The first significant change in the mass ratio can be seen in temperature range up to 200~~-~~°C, and is attributed to the loss of physisorbed water molecules, i.e. water held in ~~located at~~ micropores of the clay mineral ~~aggregate surfaces~~ (Nicolini et al., 2009), observable for both the Kaol and the Hal samples on the level of about 3%. However, with the temperature

increase up to 400 °C, a continuous mass drop of about next 3% is noted only for Hal. This is attributed to the loss of water molecules present on the internal surfaces, hence the intercalated water molecules in the interlayer space. As far as the XRD data revealed the characteristic distance for basal reflectiondiffraction of Hal at 7.4 Å, this confirms the presence of some small amount of intercalated water molecules (Moore et al., 1997). The main mass loss corresponding to structural dehydroxylationdehydroxilation of the samples occurs at ~490°C for halloysite and at ~510°C for kaolinite, which is in agreement with previously published results (Horvath et al., 2003). The TGA/DTG analysis showed also that excess thermal reactions connected to any impurities present in the samples were not detected.

3.4. TEM/SEM

The crystal size and shape are important variables because layers can be planar, curved, rolled, cylindrical or quasi-spherical (Brindley, 1980). TEM images of the Kaol sample (Figure 4) show the well-crystallized mineral with platy particles of hexagonal and/or pseudohexagonal symmetry and a lateral size ranging from 0.2 to 4.0 µm. The aspect ratio (lateral length/height) of the Kaol particles was estimated by Janek et al. (2007) to be about 5. (Janek et al., 2007). TEM images of the Hal sample (Figure 5) show that the morphology of the halloysite particles is significantly different from that of the kaolinite samples. Many irregular particles with flake shape and a high portion of tubular particles were found. The outer diameters of rolled halloysite tubes are roughly in the range 0.05 - 0.10 µm.

For comparison, SEM images show the general morphology of aggregated particles (right panel of Figure 4 and Figure 5). The SEM image of Kaol shows a typical aggregated structure made out of a few *single particles* with their edges pointing out of the image (other particles in the image lay flat on the SEM stub). The *single particle* in this study is composed of about tens layers. The Hal particles are much smaller than Kaol and they tend to form aggregates in a not clearly defined fashion. Most of the SEM micrographs of Hal showed randomly oriented

aggregates formed from many particles of different shapes as demonstrated also on the TEM images.

3.5. WAXS

Paraffin-wax (hydrocarbons with a general chemical formula C_nH_{2n+2}) is an electrically non-conductive and non-polar material with a low dielectric constant. It is used here as an alternative material to silicone oil being used as a carrier for electrorheological (ER) dispersions (see Section 3.6). Since the position of the diffuse Bragg diffraction peak from the silicone oil overlaps with the 001 Bragg reflection from both clay minerals, its use is limited. The melting temperatures of paraffin-waxes are relatively low, which make them easy to handle during the preparation of composites. In general, the solid-to-liquid transition temperature $T_{s\text{-}l}$ depends on n, which also determines the characteristic length of the paraffin chain L when in crystalline form (see Figure 6A - the strong inner ring near to the beamstop). Hence, it is important to choose an appropriate paraffin type, because the characteristic Bragg peaks from clay mineral can overlap with those from paraffin.

Figure 6B and Figure 6C show 2-D WAXS diffractograms from Hal and Kaol powders respectively. The distance $d = 2\pi / q$ between basic clay mineral layers was found to be 0.734 nm and 0.718 nm for Hal and Kaol, respectively. These basal spacing are in very good agreement with those identified in the XRD experiment (see section 3.1). As expected, different behaviour was observed for the Kaol and Hal paraffin-wax composites prepared under applied strong electric field equal to 500 V/mm. The isotropic Bragg 001 ring shown in Figure 7A points to a random orientation of Kaol particles distributed in the paraffin wax without *E*-field. However, a strong anisotropy was clearly seen in Figure 7B with the *E*-field applied during preparation of the samples. The electric field direction was horizontal and normal to the direction of the X-ray beam. This indicates that kaolinite particles were

preferentially arranged with their basal planes being parallel to the electric field direction. The quantification of the degree of anisotropy is normally achieved by fitting the azimuthal plots (Figure 7C) to a Maier-Saupe function. The fitting parameter is related to the full width at half maximum (smaller its value determine higher degree of anisotropy) and can be expressed using the standard nematic order parameter (Méheust et al., 2006; Fossum et al., 2006; Engelsberg et al., 2008; Hemmen et al., 2009; Dozov et al., 2011; Rozynek et al., 2012;). The initial Kaol/paraffin composite made without *E*-field present shows a slightly anisotropic arrangement (S_2= -0.05). This might be caused by the sample preparation procedure, since particles can align to some extent while the solution was being poured into the mould (sample cell). However, the degree of anisotropy significantly increased (7 times) after the application of electric field (S_2= -0.35).

Compared to the behaviour of kaolinite particles, the situation is very much different for Hal/paraffin composites. The WAXS results shown in Figure 8 indicate no particle alignment at all. Both the initial Hal/paraffin composite and the *E*-field treated sample present an isotropic arrangement of particles and the fitted order parameter is the same for both samples (S_2=-0.003, i.e. essentially zero).

Possible explanations for not observing any anisotropy from halloysite particles under the influence of *E*-field are: (i) particles are of different and irregular shapes, i.e. kinked tubes; (ii) large agglomerations are expected from many particles having random orientations when ~~suspended~~ dispersed in a non-polar medium; and finally (iii) halloysite particles in their present form become non-ER species, i.e. they do not re-orient, even though they become polarized under an electric field (for introduction of the non-ER concept etc., see a review on ER dispersions by Hao, 2002). The two former reasons are believed to apply here, and the justification is provided by both the electron microscopy (see Figure 4 and Figure 5) and optical microscopy measurements (see Figure 9). The particles may orient along the electric field direction, but due to their very irregular shapes, no basal plane parallel orientation (as in

the case of kaolinite particles) can be achieved. Since it is not possible to observe structuring from particles being embedded into the paraffin-wax (becomes turbid when solidifying), optical observations of particles ~~suspended~~ dispersed in silicone oil were performed.

3.6. Optical microscopy observations

The optical microscopy observations aided to exclude the hypothesis that halloysite particles make a non-ER fluid. Figure 9 shows images of both the Kaol and the Hal particles ~~suspended~~ dispersed in silicone. Randomly dispersed particles can be seen on the left panel of Figure 9, whereas two images of the particles subjected to an *E*-field of 500 V/mm are presented on the right side. The formation of chain-like structures aligning parallel to the field is clearly observed. In the case of kaolinite ER dispersion, many thin chains are visible (~10-50 μm). The particles in the halloysite ER fluid retain larger agglomerates of particles reaching nearly 200 μm. The optical observations indicate that the electrorheological properties may differ for each clay mineral dispersion, and these are presented in the next section together with the electrical current measurements.

3.7. Rheology and current response measurements

The flow curves were measured using the controlled shear rate mode for both clay/silicone oil dispersions (Figure 10). In the absence of an *E*-field, the ER fluids behave as a Newtonian fluid, i.e. their viscosities η stay constant independently of values of the shear rate $\dot{\gamma}$ (remark: two grounding brushes connected to the measuring bob induce an artificial yield stress τ of ~0.7 Pa). When a DC electric field of strengths 250, 500, 750, 1000 and 2000 V/mm were applied, the behaviour of both ER fluids changed and resembled that of a Bingham fluid, i.e. a viscoelastic material that behaves as a rigid body at low stresses but flows as a viscous fluid at high stresses. This behaviour can be described by the Bingham fluid model or its expanded form (includes the power-law index) described by the Herschel-Bulkley rheological model:

$\tau_y = \tau_y + b \cdot \dot{\gamma}^p$, where τ_y, b, p are constants named the static yield stress, the consistency index, and the power-law index, respectively. The values of the static yield stress are presented in Table 1. To compare the yield stress values presented here with that of similar systems where different types of clay minerals were used ~~(remark: the authors refer to the following publications: (~~, see Wang et al., 2009; Rozynek et al., 2010; Méheust et al., 2011.~~)~~ ~~if one wished to compare the values of the yield stresses presented here with that of similar systems where different types of clay minerals were used).~~ ~~It can be seen that t~~The ER response from the Kaol sample is significantly better and the yield stress values~~es~~ are nearly 3 times higher than those observed for the Hal sample.

So-called bifurcation tests (Bonn et al., 2002; Parmar et al., 2008; Wang et al., 2009; Khaldoun et al., 2009) were performed as a cross-check on the yield stresses determined from the controlled shear rate measurements. Two examples of such tests are shown in Figure 11. If a constant shear stress is applied to a sample, then a bifurcation in the flow curves may occur at the yield stress τ_y, indicating that microstructure re-build up is dominant if the applied stress $\tau_{ap}<\tau_y$. At high values of the applied stress on the other hand, particle re-structuring fails, e.g. $\tau_{ap}>3.35$ and $\tau_{ap}>0.8$ Pa for Kaol and Hal, respectively in the example below.

Table 1 presents ~~compares~~ the yield stresses~~es~~ values for Kaol and Hal samples measured at different electric field strengths using both mentioned methods. ~~As can be seen, t~~The values obtained from bifurcation tests coincide very well with those estimated from Herschel-Bulkley fits within experimental errors.

The values of the yield stress for the Kaol are considerably higher than those for the Hal. This behaviour can be attributed to either the differences in dielectric properties of the samples or dispersion conductivity, as this is a commonly found dependence for majority of ER-fluids. The dielectric constant of halloysite is supposed to be in general slightly higher than that of kaolinite (Churchman et al., 1975), however, the~~our~~ investigations on mica~~sceous~~

~~clays~~ using terahertz time-domain spectroscopy (THz-TDS) showed that despite significant variation in chemical composition of selected micas, the dielectric behaviour for this group of clay minerals is rather similar with the same magnitude of refractive and absorption indexes, e.g. at about 1 THz (Janek et al., 2009; Janek et al., 2010) . Taking into consideration either the polarization model or the dielectric loss model one would expect the ER response from the Kaol sample to be similar or lower. However, this is clearly not the case here. The possible validity of the conduction model, in which the conductivity mismatch between particle and liquid medium (rather than the dielectric constant mismatch) is thought to be a dominant factor for DC and low frequency alternating current (AC) excitation, was therefore tested.

The electrical conductivities of each sample were measured within the E-field range of 500 to 2000 V and the results are shown in Table 2. Since the magnitude of the DC electric conductivity I_H is significantly higher than I_K, and the conductivity mismatch Hal/silicone oil is also higher than that of Kaol/silicone oil, it can be concluded ~~we conclude~~ that the conductivity model has no direct application here either.

Both the ability of respective clay mineral to form interparticle connections and the water content adsorbed at their surface are two parameters that influence the difference between magnitudes of I_K and I_H. At the moment it is not clear which parameter is important here. However, one can postulate that the main source of conducting species in silicon-oil dispersions are the dissociated water molecules physically adsorbed at external surfaces of Kaol and on external and internal surfaces of Hal. The presence of different quantities of water was proved by TGA/DTG experiments (section 3.3). Another significant factor affecting the conductivity may be the generation of interparticle contacts after voltage application to the measuring cell. The Kaol formed highly ordered columnar structures and regular arrangement~~, in contrary to Hal~~ (Figure 9). The explanation of this different behaviour

requires more detailed current measurements as a function of e.g. particle concentration, humidity, electric field strength and time.

~~To summarize, we believed that t~~The way in which these two types of clay mineral make structures during the "chain/column" formation, as well as the concentration of available surface conducting species, seem to be ~~are~~ more important factors determining samples ER responses than the small differences between dielectric constants or material conductivity of the samples.

4. Conclusions

The structural and morphological properties of both types of clay minerals were probed in detail by means of XRD, FTIR, SEM/TEM and TGA techniques. WAXS was used to investigate the electric field induced structuring from two types of particles belonging to the kaolin group of minerals, namely kaolinite and halloysite. It was found that the overall alignment in *E*-field of the polarized kaolinite particles was significantly better compared to that of polarized halloysite particles. The authors believe that this is mainly a result of the different kind of aggregates each type of particles formed, although similar columnar final structures were made out of these aggregates in the presence of an external *E*-field. The disc-like kaolinite particles stack one another (in a coarse approximation) if immersed in a non-polar medium, and when an external *E*-field is applied such a stacked particle aligns with the *E*-field direction perpendicular to the stacking direction, which was evident in observed 2-D WAXS diffractograms. The halloysite samples were found to give no rise to anisotropy on the 2-D WAXS diffraction patterns, indicating no basal plane preferential orientation in this case. SEM and TEM images confirmed that the kaolinite sample is a well-crystallized mineral with platy particles of hexagonal symmetry, whereas the morphology of halloysite particles was found to be very different, consisting of irregular shape particles including flakes and tubular

particles. Optical microscopy was used to observe the particle alignment in the presence of the *E*-field. It was found that the electrorheological response was considerably stronger for kaolinite dispersions compared to that of the halloysites. In addition, currents at different electric field strengths were measured and it was found that the magnitude of the current was significantly larger for halloysite particles. In addition the scaling behaviour was found to be different and it is believed that the way in which these two types of clay mineral structure during the chain/column formation, as well as the concentration of available conducting species, are more important factors than the small differences between dielectric constants or material conductivity of the samples.

Acknowledgments

We wish to thank to Prof. I. Kraus (CU Bratislava, Slovakia) for his kind support of halloysite sample as well as to Mr. R. Kräuter (bene_fit Hirschau, Germany) for his kind support of kaolinite sample, which were used in the present study. We also thank to Prof. Šajgalík and Dr. Komadel for their kind agreement to perform part of the experimental work at the Institute of Inorganic Chemistry, Slovak Academy of Sciences, and Dr. J. Madejová for critical review of IR data of an earlier version of the manuscript. The assistance of Dr. Ľ. Puškelová (Geological Institute, Slovak Academy of Sciences) during XRD determination and Dr. H. Pálková during IR measurements is greatly acknowledged. The authors would also like to thank Elisabeth L. Hansen for her comments that helped to improve the manuscript. The financial support of the Slovak Grant Agency for Science VEGA (grant No. 1/4457/07), Slovak Research and Development Agency APVV (grants APVV-0491-07, VMSP-P-0110-09) and of Student Grants of CU No. UK/144/2009 is greatly appreciated. This work was supported by the Research Council of Norway through the FRINAT and CLIMIT Programs.

References

Bates, T., Hildebrand, F.A., Swineford, A., 1959. Morphology and crystal chemistry of 1:1 layer lattice silicates. American Mineralogist 35, 463-484.

~~Brindley, G.W., 1980. Order-disorder in clay mineral structures: in Crystal Structures of Clay Minerals and their X-ray Identification (G.W. Brindley and G. Brown, Ed.), 5, Mineralogical Soc., London, ch.2, 126-163.~~Brindley, G.W., Robinson, K., 1946. Randomness in the structures of kaolinitic clay minerals. Transactions of the Faraday Society 42, B198-205.

Brindley, G.W., Robinson, K., 1947. An x-ray study of some kaolinitic fireclays. Transactions of the British Ceramic Society 46, 49-62.

Brindley, G.W., Kao, C.C, Harrison, J.L., Lipsicas, M., Raythatha, R., 1986. Relation between structural disorder and other characteristics of kaolinites and dickites. Clays and Clay Minerals. 34, 239-249.

Bonn, D., Tanase, S., Abou, B., Tanaka, H., Meunier, J., 2002. Laponite: Aging and Shear Rejuvenation of a Colloidal Glass. Physical Review Letters, 89, 015701.

Chassagne, C., Mietta, F., Winterwerp, J.C., 2009. Electrokinetic study of kaolinite suspensions. Journal of Colloid and Interface Science 336, 352-359.

Cheng, H., Frost, R.L., Yang, J., Liu, Q., He, J., 2010. Thermal analysis and infrared emission spectroscopic study of halloysite–potassium acetate intercalation compound. Thermochimica Acta 511, 124–128.

Churchman, G.J., Carr, R.M., 1975. The definition and nomenclature of halloysites. Clays and Clay Minerals 23, 382-388.

Costanzo, P.M., Giese, R.F., Clemency, C.V., 1984a. Synthesis of a 10-Å hydrated kaolinite . Clays and Clay Minerals 32**,** 29-35.

Costanzo, P.M., Giese, R.F., Lipsicas, M., 1984b. Static and dynamic structure of water in hydrated kaolinites. I. The static structure. Clays and Clay Minerals 32**,** 419-428.

Costanzo, P.M., Giese, R.F., 1985. Degydration of synthetic hydrated kaolinites: a model for the dehydration of halloysite (10-Å). Clays and Clay Minerals 33, 415–423.

Dozov, I., Paineau, E., Davidson, P., Antonova, K., Baravian, C., Bihannic, I., Michot L.J., 2011. Electric-Field-Induced Perfect Anti-Nematic Order in Isotropic Aqueous Suspensions of a Natural Beidellite Clay. Journal of Physical Chemistry B 115, 7751–7765.

Engelsberg, M., de Azevedo, E.N., 2008. Diamagnetic orientation of a fluid of hard thin disks and anisotropy of the water diffusivity in the nematic phase of a suspension of clay platelets. Journal of Physical Chemistry B 112, 7045–7050.

Farmer, V.C., 2000. Transverse and longitudinal crystal modes associated with OH stretching vibrations in single crystals of kaolinite and dickite. Spectrochimica Acta A 56, 927-930.

Fossum, J.O., Méheust, Y., Parmar, K., Knudsen, K.D., Måløy, K.J., Fonseca, D., 2006. Intercalation-enhanced electric polarization and chain formation of nano-layered particles. Europhysics Letters 74, 438-444.

Gardolinski, J.E., Filho, H.P.M., Wypych, F., 2003. Thermal behavior of hydrated kaolinite. Química Nova 26, 30-35.

Giese, R.F., 1988. Kaolin Minerals: Structures and Stabilities. Review in Mineralogy and Geochemistry 19, 29-66.

Grim, R.E., 1968. Clay Mineralogy, 2nd ed., McGraw-Hill Book Company, New York, USA.

Hao, T., 2002. Electrorheological suspensions. Advances in Colloid and Interface Science 35, 1-35.

Hemmen, H., Ringdal, N.I., de Azevedo, E.N., Engelsberg, M., Hansen, E.L., Méheust, Y., Fossum, J.O., Knudsen, K.D., 2009. The Isotropic-Nematic Interface in Suspensions of Na-Fluorohectorite Synthetic Clay. Langmuir 25, 12507–12515.

Horváth, E., Frost, R.L., Makó, E., Kristóf, J., Cseh, T., 2003. Thermal treatment of mechanochemically activated kaolinite. Thermochimica Acta 404, 227-234.

Janek, M., Emmerich, K., Heissler, S., Nüesch, R. 2007. Thermally Induced Grafting Reactions of Ethylene Glycol and Glycerol Intercalates of Kaolinite. Chemistry of Materials 19, 684-693.

Janek, M., Bugár, I., Lorenc, D., Szöcs, V., Velič, D., Chorvát, D., 2009. Terahertz time-domain spectroscopy of selected layered silicates. Clays and Clay Minerals 57, 416-424.

Janek, M., Matejdes, M., Szöcs, V., Bugár, I., Gaál, A., Velič, D., Darmo, J., 2010. Dielectric properties of micaceous clays determined by terahertz time-domain spectroscopy. Philosophical Magazine **90**, 2399–2413.

Khaldoun, A., Moller, P., Fall, A., Wegdam, G., de Leeuw, B., Méheust, Y., Fossum, J.O. and Bonn, D., 2009. Quick Clay and Landslides of Clayey Soils. Physical Review Letters 103, 188301.

Lagaly, G., 1989. Principles of flow of kaolin and bentonite dispersions. Applied Clay Science 4, 105-123.

~~Madejová, J., Komadel, P., 2001. Baseline studies of the clay minerals society source clays: infrared methods. Clays and Clay Minerals 49, 410–429.~~

Madejová, J., 2003. FTIR techniques in clay mineral studies. Vibrational Spectroscopy 31, 1–10.

Madejová, J., Kraus, I., Tunega, D., Šamajová, E., 1997. Fourier transform infrared spectroscopic characterization of kaolin group minerals from the main slovak deposits. Geologica Carpathica Clays 6, 3-10.

Madejová, J., Keckes, J., Pálková, H., Komadel, P., 2002. Identification of components in smectite/kaolinite mixtures. Clay Minerals 37, 377–388.

Méheust, Y., Knudsen, K.D., Fossum, J.O., 2006. Inferring orientation distributions in anisotropic powders of nano-layered crystallites from a single two-dimensional WAXS image. Journal of Applied Crystallography 39, 661 – 670.

Méheust, Y., Parmar, K., Schjelderupsen, B., Fossum, J.O., 2011. The electrorheology of suspensions of Na-fluorohectorite clay in silicone oil. Journal of Rheology 55, 809.

Moore, D.M., Reynolds, R.C. Jr., 1997. X-ray Diffraction and the Identification and Analysis of Clay Minerals. Oxford University Press, Oxford.

Nicolini, K.P., Fukamachi, C.R.B., Wypych, F., Mangrich, A.S., 2009. Dehydrated halloysite intercalated mechanochemically with urea: Thermal behavior and structural aspects. Journal of Colloid and Interface Science 338, 474-479.

Parmar, K., Méheust, Y., Schjelderupsen, B., Fossum, J.O., 2008. Electrorheological Suspensions of Laponite in Oil: Rheometry Studies. Langmuir 24, 1814.
Rowlands, W.N., Wyndham, O´Brien R., 1995. The dynamic mobility and dielectric response of kaolinite particles. Journal of Colloid and Interface Science 175, 190 – 200.
Rozynek, Z., Wang, B., Fossum, J.O., Knudsen, K.D., 2012. Dipolar structuring of organically modified fluorohectorite clay particles. European Physical Journal E 35, 9.
Rozynek, Z., Knudsen, K.D., Fossum, J.O., Méheust, Y., Wang, B., Zhou, M., 2010. Electric field induced structuring in clay–oil suspensions: new insights from WAXS, SEM, leak current, dielectric permittivity, and rheometry. Journal of Physics: Condensed Matter 22, 324104.
Tributh, H., Lagaly, G., 1986a. *GIT Fachz.*, Lab. 30, 524 (in German).
Tributh, H., Lagaly, G., 1986b. *GIT Fachz.* Lab. 30, 771 (in German).
Wang, B., Zhou, M., Rozynek, Z., Fossum, J.O., 2009. Electrorheological properties of organically modified nanolayered laponite: influence of intercalation, adsorption and wettability. Journal of Materials Chemistry 19, 1816.

***Research Highlights**

- The structural and morphological properties of halloysite and kaolinite clays are investigated.
- Kaolinite particle dispersions have superior electro-rheological response to that of halloysite.
- Different mechanisms for the improved ER effect are tested.
- The nematic order parameter is higher for kaolinite particles dispersions.
- The magnitude of the conducting current is significantly higher for halloysite particles.

Electric-field-induced structuring and rheological properties of kaolinite and halloysite

Zbigniew Rozynek[a], Tomáš Zacher[b], Marián Janek[b], Mária Čaplovičová[c] and Jon Otto Fossum[a,d]

[a] Department of Physics, NTNU, Høgskoleringen 5, NO-7491 Trondheim, Norway
[b] Department of Physical and Theoretical Chemistry, Faculty of Natural Sciences, Comenius University, Mlynská dolina CH1, SK-84215 Bratislava, Slovakia
[c] Department of Geology of Mineral Deposits, Faculty of Natural Sciences, Comenius University, Mlynská dolina CH2, SK-84215 Bratislava, Slovakia
[d] Centre for Advanced Study at the Norwegian Academy of Science and Letters, Drammensvegen 78, 0271 Oslo, Norway

Abstract

Electric-field-induced structuring of kaolinite and halloysite particles was studied in respect to their electrorheological (ER) response in silicone oil and in paraffin dispersions. The structural and morphological properties of both clay minerals were studied by XRD, FTIR, SEM, TEM and TGA techniques. The dipolar arrangement induced under application of an electric field was investigated by 2D-WAXS and optical microscopy techniques. The ER response of the samples was measured by both the shear rate controlled method and bifurcation tests. Kaolinite particle dispersions were found to have an improved ER response relative to dispersions of halloysite particles. Finally, the electric currents of these ER fluids were measured and the results revealed differences in the current-magnitude between halloysite- and kaolinite-based silicone oil dispersions.

Keywords: kaolinite, halloysite, XRD, FTIR, electron microscopy, rheology

e-mail: zbigniew.rozynek@ntnu.no and janek@fns.uniba.sk

1. Introduction

Both kaolinite and halloysite belong to the kaolinite group of minerals having essentially similar chemical composition with the nominal formula $Al_2Si_2O_5(OH)_4$ per half unit cell, and they have important structural layer stacking differences. Natural kaolinites have various degree of structural disorder or "crystallinity", which is often related to the conditions of genesis of the particular mineral (Brindley et al., 1986; Giese, 1988; Madejová et al., 1997). Therefore, kaolinites are classified as either low defect or high defect kaolinites depending on their varying degrees of order in the crystal structure (Brindley et al., 1947). Halloysite differs intrinsically from the kaolinite in its layer stacking sequence. It can intercalate a monolayer of water molecules between the aluminosilicate layers and therefore the existence of two different mineral species of halloysite have been reported, namely the anhydrous 7 Å form and its hydrated 10 Å form, marked also as *halloysite* (*7Å*) and *halloysite* (*10Å*), respectively. The stoichiometry of halloysite (10Å) follows approximately the formula $Al_2Si_2O_5(OH)_4 \cdot 2H_2O$ per half unit cell. This hydrated form converts easily into the dehydrated form at atmospheric pressure, when dried at temperatures above 60°C, or in vacuum at room temperature. The anhydrous form with a basal spacing near 7.2 Å is metastable, and can recover its interlayer water in a wet environment. Particles of halloysite consist of tubes, rolls and cylinders, as well as irregular or spheroidal particles, whereas disc-like shapes are mainly expected for kaolinite particles. Halloysite presents a highly disordered structure, with random dislocations and shifts in both the *a* and *b* crystallographic directions (Brindley et al., 1946). The reason for the curvature of the layers is usually attributed to the lateral misfit between the octahedral and tetrahedral sheets in the structure of halloysite (Bates et al., 1959). It was postulated that stacking disorder plays an important role for hydration of kaolinite and formation of halloysite (Costanzo et al., 1984a, b). Because the 1:1 layers in hydrated

halloysite are separated from each other by a layer of water molecules, and due to higher structural disorder, halloysite have usually a larger cation exchange capacity and surface area than kaolinite (Costanzo et al., 1985; Gardolinski et al., 2003; Nicolini et al., 2009; Cheng et al., 2010).

With respect to the chemical identity but different morphology of kaolinite and halloysite particles, the effect of an electric field on electrorheological (ER) properties of silicone oil dispersions of both clay minerals have been investigated. Such investigations are important for practical utilisations of ER fluids in future mechanical coupler and/or junction devices, or in designing electrical birefringent devices. Most of the previously studied clay mineral dispersions were water-based systems. Chassagne at al. (2009) reported the electrophoretic mobility of kaolinite dispersions for different types of salt, various pH and ionic strengths; Rowlands et al. (1995) investigated the dynamic mobility and dielectric response of kaolinite particles; rheological properties of aqueous kaolinite dispersions were investigated by Lagaly (1989). However, to our knowledge, there are no data published yet for halloysite particles concerning electrokinetic response in non-polar media, and in particular not much information can be found regarding the comparison of ER behaviours of kaolinite and halloysite particles in respect to their different morphologies.

2. Samples and experimental techniques

2.1. Sample preparation

Kaolin from a primary deposit in Bayern-Oberpfalz was used in this study. The purified sample received from Hirschau, Germany, was washed with distilled water (conductivity ~1.0 μS), dried at 65°C, and crushed in an agate mortar before the characterization measurements (referred as Kaol). The halloysite sample was from a primary deposit located at Michalovce -

Biela Hora. Soluble phases of iron oxide-hydroxides were removed according to the procedure of Tributh et al. (1986a, b). This procedure includes removal of carbonates, iron oxohydroxides, organic matter such as humic material and size fractionation. The fine fraction of halloysite particles was prepared by a sedimentation method using Stoke´s equation. Collected fine particles were centrifuged, washed with distilled water (conductivity ~1.0 μS), dried at 65°C, and crushed in an agate mortar before performing the characterization measurements (referred as Hal).

For rheological measurements dispersions of Kaol and Hal in silicone oil (~5 m%) were prepared by mixing in an orbital shaker for minimum 12 hours and applying 30 minutes of ultrasonication prior to each rheological and current measurement.

Kaol/paraffin and Hal/paraffin composites were prepared (instead of silicone oil-based dispersions) for wide-angle X-ray scattering (WAXS) experiments, since the position of a diffuse Bragg diffraction peak from silicone oil overlaps with the 001 Bragg reflection from both clay minerals. The composites were prepared as following: 1.4 g of each clay mineral powder was slowly added into 7g of already pre-melted paraffin-wax (120-130°C). After vigorous stirring, the dispersions were left undisturbed for 5 minutes to let the largest aggregates sediment and then the top portion (80 %) was poured into a new 10 ml glass vial. The dispersions were kept at ~125°C under stirring. After 2 hours four samples were prepared and these included: Kaol/paraffin and Hal/paraffin composites cast with and without *E*-field present. After the samples solidified, having a form of stripes (~15 x 6.5 x 1.5 mm), the WAXS measurements were performed. Optical microscopy measurements were done using low concentration (below 0.5 m%) clay mineral in oil dispersions (for observation clarity).

2.2. Experimental techniques

2.2.1. XRD

X-ray diffraction (XRD) patterns from kaolinite and halloysite powders were obtained using a PHILIPS PW 1710 X-ray powder diffractometer equipped with a Graphite monochromator PW 1752 and Cu radiation ($CuK\alpha_1$ λ=0.154056 nm). The patterns were scanned in the range of 4-70° in 2θ with a step size of 0.02° and a counting time of 2.0 s/step.

2.2.2. FTIR

Infrared spectra of the Kaol and Hal samples were obtained using a Nicolet 6700 Fourier Transform Infrared (FTIR) spectrometer from Thermo Scientific. The KBr pressed disk technique (0.5 mg of sample and 200 mg KBr) was used to get spectra in the MIR region (4000–400cm^{-1}). The discs were heated in a furnace overnight at 130°C to minimize the water adsorbed on KBr and the clay mineral sample. For each sample 128 scans with the resolution of 4 cm^{-1} were recorded. Spectra manipulations were performed using the Thermo Scientific OMNIC^{TM} software package.

2.2.3. TGA

Thermal gravimetric analysis (TGA) was performed on a TGA/SDTA851^{e} instrument (Mettler Toledo As.) with a heating rate of 2ºC/min up to 800°C under static air conditions. About 20 mg of sample was supplied to the Alumina crucible (with no lid covered).

2.2.4. TEM/SEM

Transmission electron microscopy (TEM) images of Kaol and Hal were recorded on a JEOL JEM-2000FX transmission electron microscope with an accelerating voltage of 160 kV. For this characterization the samples were prepared as follows: Kaol and Hal ethanol dispersions were treated 5 minutes by ultrasounds. Then a drop of the sample was spilled on a copper reticle coated colloidal film with a layer of carbon and finally the sample was dried at room temperature.

Scanning electron micrographs (SEM) were acquired using a field emission scanning electron microscope (Zeiss Ultra, 55 Limited Edition, accelerated voltage 10-15kV). For the

SEM samples, a dispersion of a small amount (<0.01 m%) of sample was dispersed in de-ionized water and ultrasonicated for 1 hour, and then pipetted onto a SEM stub. Before images were collected, all samples were carbon-coated in a conventional coating unit.

2.2.5. WAXS

The WAXS experiment was carried out at the European Synchrotron Radiation Facility (ESRF) in Grenoble, France. An X-ray beam with a wavelength of 0.9 Å and a 0.5 × 0.5 mm^2 beam size at the sample was used. The Swiss-Norwegian beamline (SNBL) BM01A is equipped with a two-dimensional MAR345 image plate detector with a diameter of 345 mm. The sample to detector distance was set to 350 mm, enabling the detection of scattering in a *q*-range of approximately 0.65 – 17 nm^{-1}, which corresponds to the real space *d*-range of 0.37 – 10 nm.

2.2.6. Rheometry and current measurements

The rheological properties of the clay mineral dispersions were measured under direct current (DC) electric fields using a Physica MCR300 Rotational Rheometer equipped with a coaxial cylinder (Physica ERD CC/27). All the rheological measurements were performed at constant temperature of 23°C. These included controlled shear rate tests for measuring shear stress as a function of shear rate and bifurcation measurements. In the former experiment the so-called flow curves were collected in the shear rate range between 0.1 and 1000 s^{-1} and fitted to Herschel–Bulkley model in order to obtain the static yield stresses for samples at different *E*-field strengths, namely 250, 500, 750, 1000, 1500 and 2000 V/mm, respectively. The bifurcation tests were performed as a complementary method to verify the values of the yield stresses. In this method samples were forced to flow under a constant stress, and then let to evolve in the presence of an *E*-field (see details in section 3.7). In addition, current

measurements were performed (in the same rheological cell) using an Agilent 34401A multimeter.

3. Results and discussion

3.1. XRD analysis

The structural and morphological properties of layered clay minerals can be indirectly deduced from their diffraction patterns. XRD patterns of both samples are shown in Figure 1A. The transition from the sharp diffraction peaks in Kaol to the mainly diffuse and "tailed" reflections in the pattern of Hal are shown, indicating decreased layer stacking order of the Hal sample. The *d*-spacing of the first basal reflections are 0.71 nm and 0.74 nm, for Kaol and Hal respectively. We suppose that an almost anhydrous form of halloysite was used in the experiments. The group of reflections from 020 to 002 particularly reflects the change of structural disorder. In this region the clearly resolved doublet $1\bar{1}1$ and $1\bar{1}\bar{1}$ of the Kaol sample yields a single broadened reflection for the Hal sample (Figure 1B). This represents evidence for the increase in structural disorder for Hal (Grim, 1968).

3.2. FTIR spectroscopy.

FTIR was used as a complementary method to the XRD to investigate possible mineral admixtures in the samples. Well-ordered Kaol samples revealed four clearly-resolved absorption bands in the OH stretching region 3693-3620 cm^{-1} (Figure 2). A strong band at 3696 cm^{-1} is related to the in-phase symmetric stretching vibration, two weak absorptions at 3668 and 3652 cm^{-1} are assigned to out-of-plane stretching vibrations (Farmer, 2000; Madejová et al., 2002). In contrary, the IR spectrum of Hal shows intensive absorption bands only at 3696 and 3621 cm^{-1} in the OH stretching region. The very low intensity of OH

187 stretching bands at 3671 and 3652 cm^{-1} reflect a poorly ordered structure typical for halloysite
188 samples (Brindley et al., 1947).
189 Structural stretching and bending as well as OH bending absorption bands are in the region
190 1300–400 cm^{-1} (Figure 2). Differences in layer stacking arrangement of the basic layers are
191 reflected in the positions and shape of the bands. Clear differences between Kaol and Hal can
192 be seen in the 1300-400 cm^{-1} region. The AlAlOH bending bands at 937 and 912 cm^{-1} for
193 Kaol are detected as a shoulder near 939 cm^{-1} and as a distinct band at 913 cm^{-1} for Hal. The
194 band at 430 cm^{-1} was observed in both Kaol and Hal spectra and belongs to Si-O deformation
195 vibrations (Madejová et al., 2002). The inset in Figure 2 shows the details of OH stretching
196 bands located at 3654 and 3649 cm^{-1}. These are typical wavelengths for OH vibrations from
197 kaolinite, thus a small fraction of kaolinite-like particles is expected to be present in the Hal
198 sample. However, no other mineral admixtures or impurities were detected by the FTIR
199 technique.
200
201 **3.3. TGA/DTG**
202 TGA was conducted mainly to prove the mineral purity and water content in both minerals.
203 Figure 3 shows typical TGA/DTG behaviour of both the Kaol and the Hal samples in the
204 temperature window 50-800°C.
205 The first significant change in the mass ratio can be seen in temperature range up to 200°C,
206 and is attributed to the loss of physisorbed water molecules, i.e. water held in micropores of
207 the clay mineral(Nicolini et al., 2009), observable for both the Kaol and the Hal samples on
208 the level of about 3%. However, with the temperature increase up to 400°C, a continuous
209 mass drop of about next 3% is noted only for Hal. This is attributed to the loss of intercalated
210 water molecules in the interlayer space. As far as the XRD data revealed the characteristic
211 distance for basal reflection of Hal at 7.4 Å, this confirms the presence of some small amount

of intercalated water molecules (Moore et al., 1997). The main mass loss corresponding to structural dehydroxylation of the samples occurs at ~490°C for halloysite and at ~510°C for kaolinite, which is in agreement with previously published results (Horvath et al., 2003).

3.4. TEM/SEM

TEM images of the Kaol sample (Figure 4) show the well-crystallized mineral with platy particles of hexagonal and/or pseudohexagonal symmetry and a lateral size ranging from 0.2 to 4.0 μm. The aspect ratio (lateral length/height) of the Kaol particles was estimated by Janek et al. (2007) to be about 5. TEM images of the Hal sample (Figure 5) show that the morphology of the halloysite particles is significantly different from that of the kaolinite samples. Many irregular particles with flake shape and a high portion of tubular particles were found. The outer diameters of rolled halloysite tubes are roughly in the range 0.05 - 0.10 μm.

For comparison, SEM images show the general morphology of aggregated particles (right panel of Figure 4 and Figure 5). The SEM image of Kaol shows a typical aggregated structure made out of a few *single particles* with their edges pointing out of the image (other particles in the image lay flat on the SEM stub). The *single particle* in this study is composed of about tens layers. The Hal particles are much smaller than Kaol and they tend to form aggregates in a not clearly defined fashion. Most of the SEM micrographs of Hal showed randomly oriented aggregates formed from many particles of different shapes as demonstrated also on the TEM images.

3.5. WAXS

Paraffin-wax (hydrocarbons with a general chemical formula C_nH_{2n+2}) is an electrically non-conductive and non-polar material with a low dielectric constant. It is used here as an alternative material to silicone oil being used as a carrier for electrorheological (ER) dispersions (see Section 3.6). Since the position of the diffuse Bragg diffraction peak from the

238 silicone oil overlaps with the 001 Bragg reflection from both clay minerals, its use is limited.
239 The melting temperatures of paraffin-waxes are relatively low, which make them easy to
240 handle during the preparation of composites. In general, the solid-to-liquid transition
241 temperature $T_{s\text{-}l}$ depends on *n*, which also determines the characteristic length of the paraffin
242 chain *L* when in crystalline form (see Figure 6A - the strong inner ring near to the beamstop).
243 Hence, it is important to choose an appropriate paraffin type, because the characteristic Bragg
244 peaks from clay mineral can overlap with those from paraffin.

245 Figure 6B and Figure 6C show 2-D WAXS diffractograms from Hal and Kaol powders
246 respectively. The distance $d = 2\pi / q$ between basic clay mineral layers was found to be
247 0.734 nm and 0.718 nm for Hal and Kaol, respectively. These basal spacing are in very good
248 agreement with those identified in the XRD experiment (see section 3.1). As expected,
249 different behaviour was observed for the Kaol and Hal paraffin-wax composites prepared
250 under applied strong electric field equal to 500 V/mm. The isotropic Bragg 001 ring shown in
251 Figure 7A points to a random orientation of Kaol particles distributed in the paraffin wax
252 without *E*-field. However, a strong anisotropy was clearly seen in Figure 7B with the *E*-field
253 applied during preparation of the samples. The electric field direction was horizontal and
254 normal to the direction of the X-ray beam. This indicates that kaolinite particles were
255 preferentially arranged with their basal planes being parallel to the electric field direction. The
256 quantification of the degree of anisotropy is normally achieved by fitting the azimuthal plots
257 (Figure 7C) to a Maier-Saupe function. The fitting parameter is related to the full width at half
258 maximum (smaller its value determine higher degree of anisotropy) and can be expressed
259 using the standard nematic order parameter (Méheust et al., 2006; Fossum et al., 2006;
260 Engelsberg et al., 2008; Hemmen et al., 2009; Dozov et al., 2011; Rozynek et al., 2012;).
261 The initial Kaol/paraffin composite made without *E*-field present shows a slightly anisotropic
262 arrangement (S_2= -0.05). This might be caused by the sample preparation procedure, since

particles can align to some extent while the solution was being poured into the mould (sample cell). However, the degree of anisotropy significantly increased (7 times) after the application of electric field (S_2= -0.35).

Compared to the behaviour of kaolinite particles, the situation is very much different for Hal/paraffin composites. The WAXS results shown in Figure 8 indicate no particle alignment at all. Both the initial Hal/paraffin composite and the *E*-field treated sample present an isotropic arrangement of particles and the fitted order parameter is the same for both samples (S_2=-0.003, i.e. essentially zero).

Possible explanations for not observing any anisotropy from halloysite particles under the influence of *E*-field are: (i) particles are of different and irregular shapes, i.e. kinked tubes; (ii) large agglomerations are expected from many particles having random orientations when dispersed in a non-polar medium; and finally (iii) halloysite particles in their present form become non-ER species, i.e. they do not re-orient, even though they become polarized under an electric field (for introduction of the non-ER concept etc., see a review on ER dispersions by Hao, 2002). The two former reasons are believed to apply here, and the justification is provided by both the electron microscopy (see Figure 4 and Figure 5) and optical microscopy measurements (see Figure 9). The particles may orient along the electric field direction, but due to their very irregular shapes, no basal plane parallel orientation (as in the case of kaolinite particles) can be achieved. Since it is not possible to observe structuring from particles being embedded into the paraffin-wax (becomes turbid when solidifying), optical observations of particles dispersed in silicone oil were performed.

3.6. Optical microscopy observations

The optical microscopy observations aided to exclude the hypothesis that halloysite particles make a non-ER fluid. Figure 9 shows images of both the Kaol and the Hal particles dispersed in silicone. Randomly dispersed particles can be seen on the left panel of Figure 9,

whereas two images of the particles subjected to an *E*-field of 500 V/mm are presented on the right side. The formation of chain-like structures aligning parallel to the field is clearly observed. In the case of kaolinite ER dispersion, many thin chains are visible (~10-50 μm). The particles in the halloysite ER fluid retain larger agglomerates of particles reaching nearly 200 μm. The optical observations indicate that the electrorheological properties may differ for each clay mineral dispersion, and these are presented in the next section together with the electrical current measurements.

3.7. Rheology and current response measurements

The flow curves were measured using the controlled shear rate mode for both clay/silicone oil dispersions (Figure 10). In the absence of an *E*-field, the ER fluids behave as a Newtonian fluid, i.e. their viscosities η stay constant independently of values of the shear rate $\dot{\gamma}$ (remark: two grounding brushes connected to the measuring bob induce an artificial yield stress τ of ~0.7 Pa). When a DC electric field of strengths 250, 500, 750, 1000 and 2000 V/mm were applied, the behaviour of both ER fluids changed and resembled that of a Bingham fluid, i.e. a viscoelastic material that behaves as a rigid body at low stresses but flows as a viscous fluid at high stresses. This behaviour can be described by the Bingham fluid model or its expanded form (includes the power-law index) described by the Herschel-Bulkley rheological model: $\tau_y = \tau_y + b \cdot \dot{\gamma}^p$, where τ_y, b, p are constants named the static yield stress, the consistency index, and the power-law index, respectively. The values of the static yield stress are presented in Table 1. To compare the yield stress values presented here with that of similar systems where different types of clay minerals were used , see Wang et al., 2009; Rozynek et al., 2010; Méheust et al., 2011. The ER response from the Kaol sample is significantly better and the yield stress values are nearly 3 times higher than those observed for the Hal sample.

So-called bifurcation tests (Bonn et al., 2002; Parmar et al., 2008; Wang et al., 2009; Khaldoun et al., 2009) were performed as a cross-check on the yield stresses determined from the controlled shear rate measurements. Two examples of such tests are shown in Figure 11. If a constant shear stress is applied to a sample, then a bifurcation in the flow curves may occur at the yield stress τ_y, indicating that microstructure re-build up is dominant if the applied stress $\tau_{ap}<\tau_y$. At high values of the applied stress on the other hand, particle re-structuring fails, e.g. $\tau_{ap}>3.35$ and $\tau_{ap}>0.8$ Pa for Kaol and Hal, respectively in the example below.

Table 1 presents the yield stress values for Kaol and Hal samples measured at different electric field strengths using both mentioned methods. The values obtained from bifurcation tests coincide very well with those estimated from Herschel-Bulkley fits within experimental errors.

The values of the yield stress for the Kaol are considerably higher than those for the Hal. This behaviour can be attributed to either the differences in dielectric properties of the samples or dispersion conductivity, as this is a commonly found dependence for majority of ER-fluids. The dielectric constant of halloysite is supposed to be in general slightly higher than that of kaolinite (Churchman et al., 1975), however, the investigations on micas using terahertz time-domain spectroscopy (THz-TDS) showed that despite significant variation in chemical composition of selected micas, the dielectric behaviour for this group of clay minerals is rather similar with the same magnitude of refractive and absorption indexes, e.g. at about 1 THz (Janek et al., 2009; Janek et al., 2010) . Taking into consideration either the polarization model or the dielectric loss model one would expect the ER response from the Kaol sample to be similar or lower. However, this is clearly not the case here. The possible validity of the conduction model, in which the conductivity mismatch between particle and liquid medium (rather than the dielectric constant mismatch) is thought to be a dominant factor for DC and low frequency alternating current (AC) excitation, was therefore tested.

The electrical conductivities of each sample were measured within the E-field range of 500 to 2000 V and the results are shown in Table 2. Since the magnitude of the DC electric conductivity I_H is significantly higher than I_K, and the conductivity mismatch Hal/silicone oil is also higher than that of Kaol/silicone oil, it can be concluded that the conductivity model has no direct application here either.

Both the ability of respective clay mineral to form interparticle connections and the water content adsorbed at their surface are two parameters that influence the difference between magnitudes of I_K and I_H. At the moment it is not clear which parameter is important here. However, one can postulate that the main source of conducting species in silicon-oil dispersions are the dissociated water molecules physically adsorbed at external surfaces of Kaol and on external and internal surfaces of Hal. The presence of different quantities of water was proved by TGA/DTG experiments (section 3.3). Another significant factor affecting the conductivity may be the generation of interparticle contacts after voltage application to the measuring cell. The Kaol formed highly ordered columnar structures and regular arrangement (Figure 9). The explanation of this different behaviour requires more detailed current measurements as a function of e.g. particle concentration, humidity, electric field strength and time.

The way in which these two types of clay mineral make structures during the "chain/column" formation, as well as the concentration of available surface conducting species, seem to be more important factors determining samples ER responses than the small differences between dielectric constants or material conductivity of the samples.

4. Conclusions

The structural and morphological properties of both types of clay minerals were probed in detail by means of XRD, FTIR, SEM/TEM and TGA techniques. WAXS was used to

investigate the electric field induced structuring from two types of particles belonging to the kaolin group of minerals, namely kaolinite and halloysite. It was found that the overall alignment in *E*-field of the polarized kaolinite particles was significantly better compared to that of polarized halloysite particles. The authors believe that this is mainly a result of the different kind of aggregates each type of particles formed, although similar columnar final structures were made out of these aggregates in the presence of an external *E*-field. The disc-like kaolinite particles stack one another (in a coarse approximation) if immersed in a non-polar medium, and when an external *E*-field is applied such a stacked particle aligns with the *E*-field direction perpendicular to the stacking direction, which was evident in observed 2-D WAXS diffractograms. The halloysite samples were found to give no rise to anisotropy on the 2-D WAXS diffraction patterns, indicating no basal plane preferential orientation in this case. SEM and TEM images confirmed that the kaolinite sample is a well-crystallized mineral with platy particles of hexagonal symmetry, whereas the morphology of halloysite particles was found to be very different, consisting of irregular shape particles including flakes and tubular particles. Optical microscopy was used to observe the particle alignment in the presence of the *E*-field. It was found that the electrorheological response was considerably stronger for kaolinite dispersions compared to that of the halloysites. In addition, currents at different electric field strengths were measured and it was found that the magnitude of the current was significantly larger for halloysite particles. In addition the scaling behaviour was found to be different and it is believed that the way in which these two types of clay mineral structure during the chain/column formation, as well as the concentration of available conducting species, are more important factors than the small differences between dielectric constants or material conductivity of the samples.

Acknowledgments

We wish to thank to Prof. I. Kraus (CU Bratislava, Slovakia) for his kind support of halloysite sample as well as to Mr. R. Kräuter (bene_fit Hirschau, Germany) for his kind support of kaolinite sample, which were used in the

present study. We also thank to Prof. Šajgalík and Dr. Komadel for their kind agreement to perform part of the experimental work at the Institute of Inorganic Chemistry, Slovak Academy of Sciences, and Dr. J. Madejová for critical review of IR data of an earlier version of the manuscript. The assistance of Dr. Ľ. Puškelová (Geological Institute, Slovak Academy of Sciences) during XRD determination and Dr. H. Pálková during IR measurements is greatly acknowledged. The authors would also like to thank Elisabeth L. Hansen for her comments that helped to improve the manuscript. The financial support of the Slovak Grant Agency for Science VEGA (grant No. 1/4457/07), Slovak Research and Development Agency APVV (grants APVV-0491-07, VMSP-P-0110-09) and of Student Grants of CU No. UK/144/2009 is greatly appreciated. This work was supported by the Research Council of Norway through the FRINAT and CLIMIT Programs.

References

Bates, T., Hildebrand, F.A., Swineford, A., 1959. Morphology and crystal chemistry of 1:1 layer lattice silicates. American Mineralogist 35, 463-484.

Brindley, G.W., Robinson, K., 1946. Randomness in the structures of kaolinitic clay minerals. Transactions of the Faraday Society 42, B198-205.

Brindley, G.W., Robinson, K., 1947. An x-ray study of some kaolinitic fireclays. Transactions of the British Ceramic Society 46, 49-62.

Brindley, G.W., Kao, C.C, Harrison, J.L., Lipsicas, M., Raythatha, R., 1986. Relation between structural disorder and other characteristics of kaolinites and dickites. Clays and Clay Minerals. 34, 239-249.

Bonn, D., Tanase, S., Abou, B., Tanaka, H., Meunier, J., 2002. Laponite: Aging and Shear Rejuvenation of a Colloidal Glass. Physical Review Letters, 89, 015701.

Chassagne, C., Mietta, F., Winterwerp, J.C., 2009. Electrokinetic study of kaolinite suspensions. Journal of Colloid and Interface Science 336, 352-359.

Cheng, H., Frost, R.L., Yang, J., Liu, Q., He, J., 2010. Thermal analysis and infrared emission spectroscopic study of halloysite–potassium acetate intercalation compound. Thermochimica Acta 511, 124–128.

Churchman, G.J., Carr, R.M., 1975. The definition and nomenclature of halloysites. Clays and Clay Minerals 23, 382-388.

Costanzo, P.M., Giese, R.F., Clemency, C.V., 1984a. Synthesis of a 10-Å hydrated kaolinite . Clays and Clay Minerals 32**,** 29-35.

Costanzo, P.M., Giese, R.F., Lipsicas, M., 1984b. Static and dynamic structure of water in hydrated kaolinites. I. The static structure. Clays and Clay Minerals 32**,** 419-428.

Costanzo, P.M., Giese, R.F., 1985. Degydration of synthetic hydrated kaolinites: a model for the dehydration of halloysite (10-Å). Clays and Clay Minerals 33, 415–423.

Dozov, I., Paineau, E., Davidson, P., Antonova, K., Baravian, C., Bihannic, I., Michot L.J., 2011. Electric-Field-Induced Perfect Anti-Nematic Order in Isotropic Aqueous Suspensions of a Natural Beidellite Clay. Journal of Physical Chemistry B 115, 7751–7765.

Engelsberg, M., de Azevedo, E.N., 2008. Diamagnetic orientation of a fluid of hard thin disks and anisotropy of the water diffusivity in the nematic phase of a suspension of clay platelets. Journal of Physical Chemistry B 112, 7045–7050.

Farmer, V.C., 2000. Transverse and longitudinal crystal modes associated with OH stretching vibrations in single crystals of kaolinite and dickite. Spectrochimica Acta A 56, 927-930.

Fossum, J.O., Méheust, Y., Parmar, K., Knudsen, K.D., Måløy, K.J., Fonseca, D., 2006. Intercalation-enhanced electric polarization and chain formation of nano-layered particles. Europhysics Letters 74, 438-444.

Gardolinski, J.E., Filho, H.P.M., Wypych, F., 2003. Thermal behavior of hydrated kaolinite. Química Nova 26, 30-35.

Giese, R.F., 1988. Kaolin Minerals: Structures and Stabilities. Review in Mineralogy and Geochemistry 19, 29-66.

Grim, R.E., 1968. Clay Mineralogy, 2nd ed., McGraw-Hill Book Company, New York, USA.

Hao, T., 2002. Electrorheological suspensions. Advances in Colloid and Interface Science 35, 1-35.

Hemmen, H., Ringdal, N.I., de Azevedo, E.N., Engelsberg, M., Hansen, E.L., Méheust, Y., Fossum, J.O., Knudsen, K.D., 2009. The Isotropic-Nematic Interface in Suspensions of Na-Fluorohectorite Synthetic Clay. Langmuir 25, 12507–12515.

Horváth, E., Frost, R.L., Makó, E., Kristóf, J., Cseh, T., 2003. Thermal treatment of mechanochemically activated kaolinite. Thermochimica Acta 404, 227-234.

Janek, M., Emmerich, K., Heissler, S., Nüesch, R. 2007. Thermally Induced Grafting Reactions of Ethylene Glycol and Glycerol Intercalates of Kaolinite. Chemistry of Materials 19, 684-693.

Janek, M., Bugár, I., Lorenc, D., Szöcs, V., Velič, D., Chorvát, D., 2009. Terahertz time-domain spectroscopy of selected layered silicates. Clays and Clay Minerals 57, 416-424.

Janek, M., Matejdes, M., Szöcs, V., Bugár, I., Gaál, A., Velič, D., Darmo, J., 2010. Dielectric properties of micaceous clays determined by terahertz time-domain spectroscopy. Philosophical Magazine **90**, 2399–2413.

Khaldoun, A., Moller, P., Fall, A., Wegdam, G., de Leeuw, B., Méheust, Y., Fossum, J.O. and Bonn, D., 2009. Quick Clay and Landslides of Clayey Soils. Physical Review Letters 103, 188301.

Lagaly, G., 1989. Principles of flow of kaolin and bentonite dispersions. Applied Clay Science 4, 105-123.

Madejová, J., 2003. FTIR techniques in clay mineral studies. Vibrational Spectroscopy 31, 1–10.

Madejová, J., Kraus, I., Tunega, D., Šamajová, E., 1997. Fourier transform infrared spectroscopic characterization of kaolin group minerals from the main slovak deposits. Geologica Carpathica Clays 6, 3-10.

Madejová, J., Keckes, J., Pálková, H., Komadel, P., 2002. Identification of components in smectite/kaolinite mixtures. Clay Minerals 37, 377–388.

Méheust, Y., Knudsen, K.D., Fossum, J.O., 2006. Inferring orientation distributions in anisotropic powders of nano-layered crystallites from a single two-dimensional WAXS image. Journal of Applied Crystallography 39, 661 – 670.

Méheust, Y., Parmar, K., Schjelderupsen, B., Fossum, J.O., 2011. The electrorheology of suspensions of Na-fluorohectorite clay in silicone oil. Journal of Rheology 55, 809.

Moore, D.M., Reynolds, R.C. Jr., 1997. X-ray Diffraction and the Identification and Analysis of Clay Minerals. Oxford University Press, Oxford.

Nicolini, K.P., Fukamachi, C.R.B., Wypych, F., Mangrich, A.S., 2009. Dehydrated halloysite intercalated mechanochemically with urea: Thermal behavior and structural aspects. Journal of Colloid and Interface Science 338, 474-479.

Parmar, K., Méheust, Y., Schjelderupsen, B., Fossum, J.O., 2008. Electrorheological Suspensions of Laponite in Oil: Rheometry Studies. Langmuir 24, 1814.

Rowlands, W.N., Wyndham, O´Brien R., 1995. The dynamic mobility and dielectric response of kaolinite particles. Journal of Colloid and Interface Science 175, 190 – 200.

469 Rozynek, Z., Wang, B., Fossum, J.O., Knudsen, K.D., 2012. Dipolar structuring of organically modified fluorohectorite clay
470 particles. European Physical Journal E 35, 9.
471 Rozynek, Z., Knudsen, K.D., Fossum, J.O., Méheust, Y., Wang, B., Zhou, M., 2010. Electric field induced structuring in
472 clay–oil suspensions: new insights from WAXS, SEM, leak current, dielectric permittivity, and rheometry. Journal of
473 Physics: Condensed Matter 22, 324104.
474 Tributh, H., Lagaly, G., 1986a. *GIT Fachz.*, Lab. 30, 524 (in German).
475 Tributh, H., Lagaly, G., 1986b. *GIT Fachz.* Lab. 30, 771 (in German).
476 Wang, B., Zhou, M., Rozynek, Z., Fossum, J.O., 2009. Electrorheological properties of organically modified nanolayered
477 laponite: influence of intercalation, adsorption and wettability. Journal of Materials Chemistry 19, 1816.
478

Table 1
Click here to download Table: Table 1.doc

E-field [V/mm]		250	500	750	1000	2000
τ_y [Pa]	Kaol (CSR)	1.7 ± 0.4	3.6 ± 0.1	5.2 ± 0.3	10.2 ± 0.4	18.5 ± 1.3
τ_y [Pa]	Kaol (bif.)	1.5 ± 0.5	3.3 ± 0.1	5.5 ± 0.5	9.5 ± 0.5	16.5 ± 0.5
τ_y [Pa]	Hal (CSR)	0.9 ± 0.8	1.3 ± 0.5	1.6 ± 0.9	1.9 ± 0.8	6.3 ± 1.1
τ_y [Pa]	Hal (bif.)	0.6 ± 0.1	0.9 ± 0.1	1.5 ± 0.5	2.5 ± 0.5	7.5 ± 0.5

Table 1. Comparison of the yield stresses for Kaol and Hal dispersions measured at different *E*-field strengths employing constant shear rate (CSR) and bifurcation (bif.) methods.

Table 2

Click here to download Table: Table 2.doc

E-field [V/mm]		500	750	1000	1250	1500	1750	2000
I [µA]	Kaol	0.6	1.5	2.9	4.9	7.5	11	15
I [µA]	Hal	34	59	91	132	181	238	305

Table 2. Comparison of DC currents for Kaol and Hal dispersions measured at different *E*-field strengths.

Figure 1

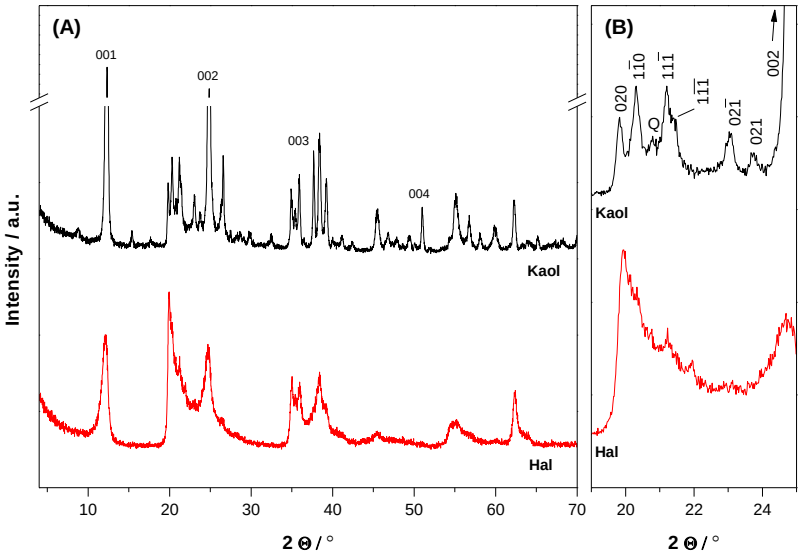

Fig. 1. The XRD patterns of Kaol and Hal samples with indicated basal reflections.

Figure 2

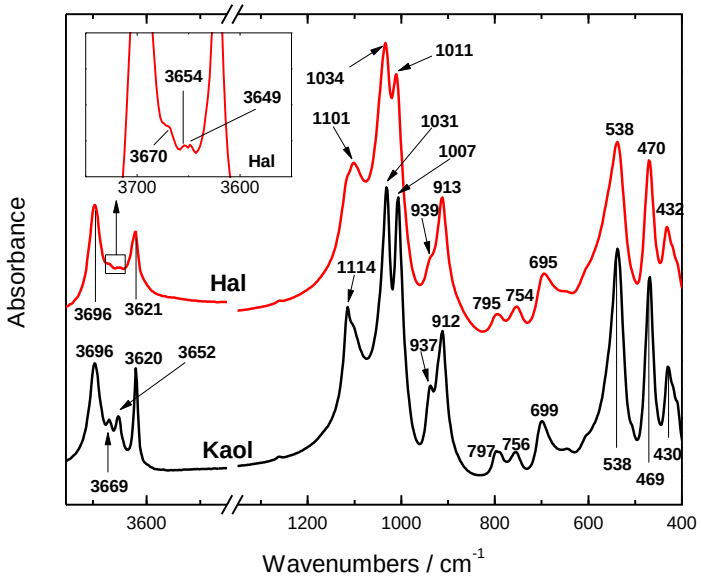

Fig. 2. FTIR spectra of Kaol and Hal samples.

Figure 3

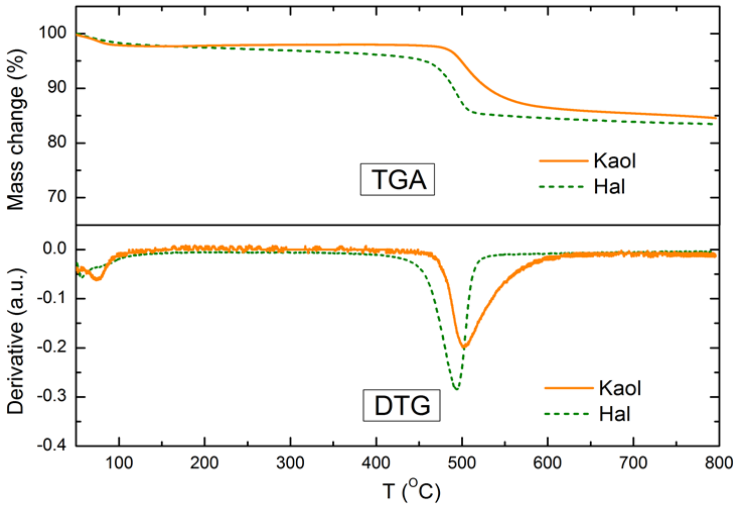

Fig. 3. TGA and DTG traces (50-800°C) of Kaol (solid) and Hal (dashed) samples.

Figure 4 and 5

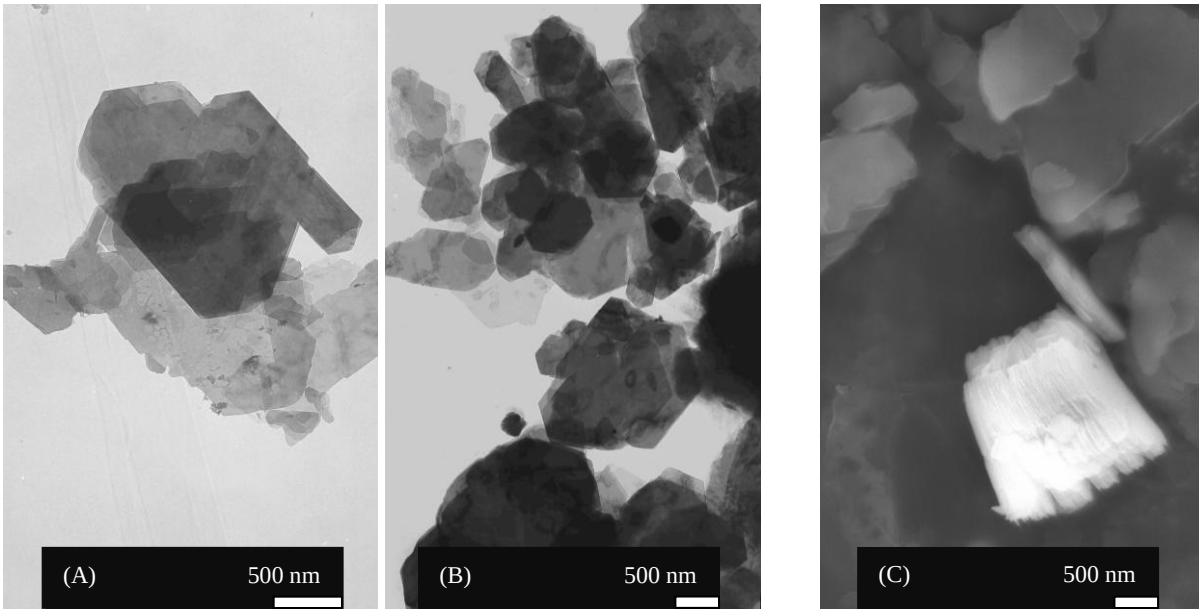

Fig. 4. The Kaol particles' shape and size distribution can be determined from TEM (A,B) micrographs. The SEM (C) image shows the Kaol typical aggregated structure made out of few single particles.

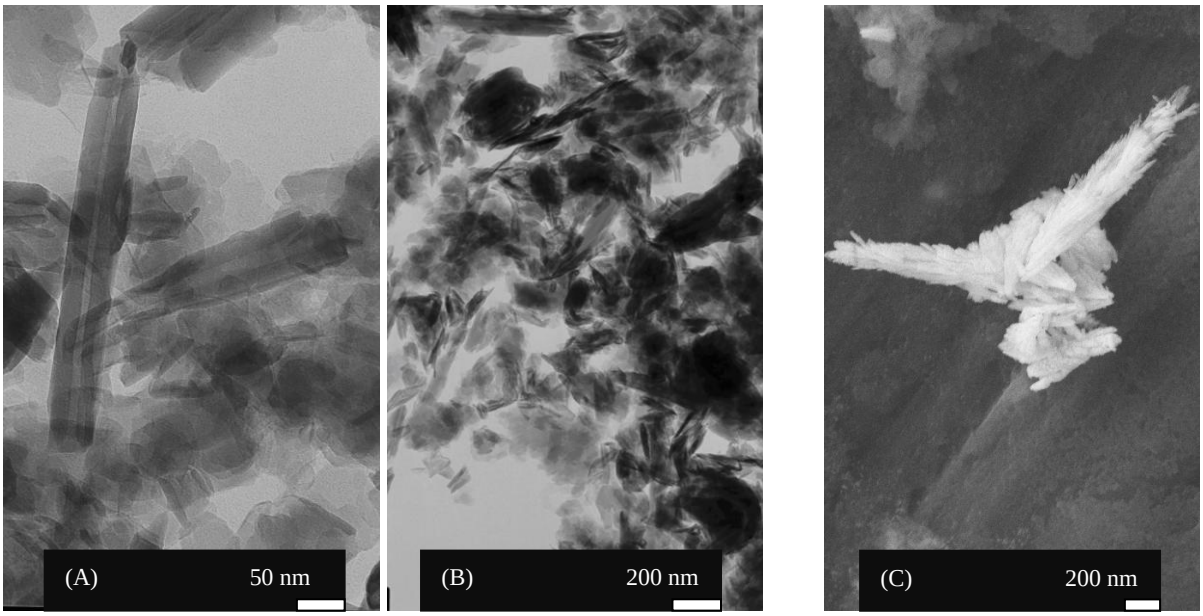

Fig. 5. The Hal particles' shape and size distribution can be determined from TEM (A,B) micrographs. The SEM (C) image shows the Hal undefined aggregated structure made out many small tubular single particles.

.

Figure 6

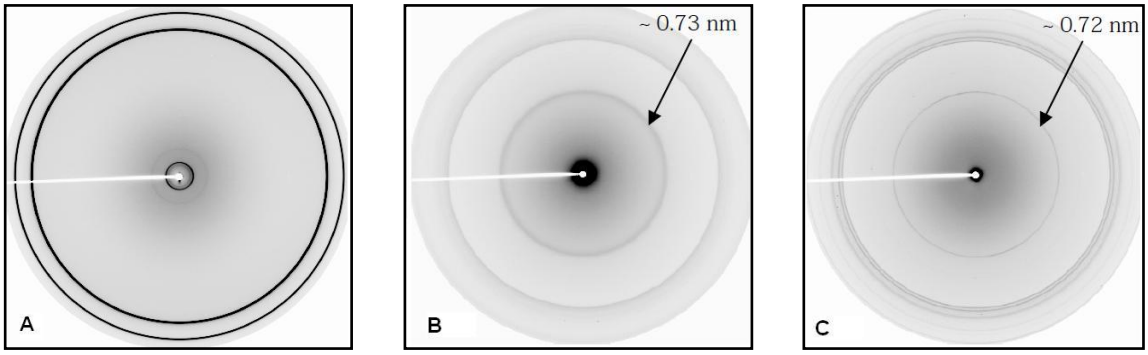

Fig. 6. WAXS 2-D images of pure paraffin-wax (A), Hal powder (B) and Kaol powder (C).

Figure 7

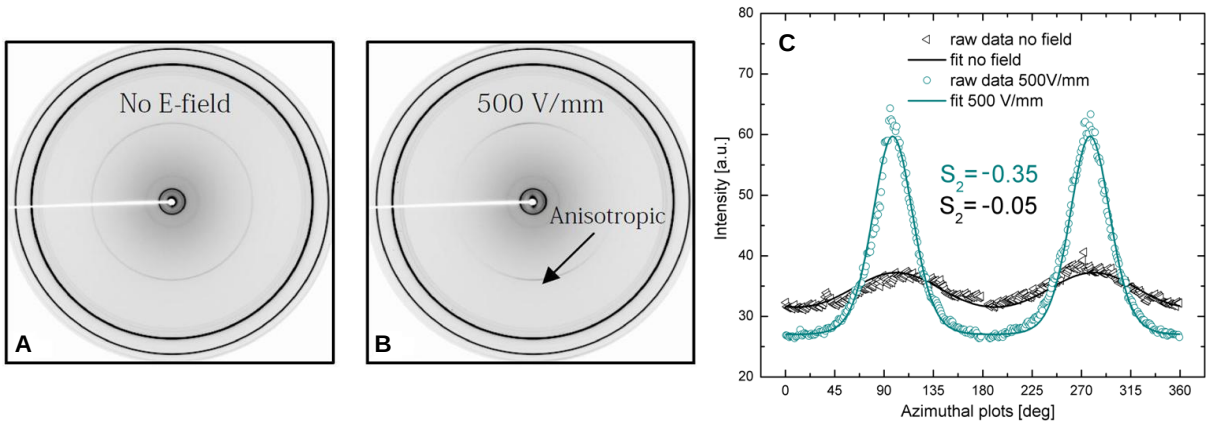

Fig. 7. WAXS 2-D images of Kaol/paraffin composite without (A) and with (B) *E*-field of 500 V/mm. Azimuthal plots with calculated nematic order parameter (C).

Figure 8

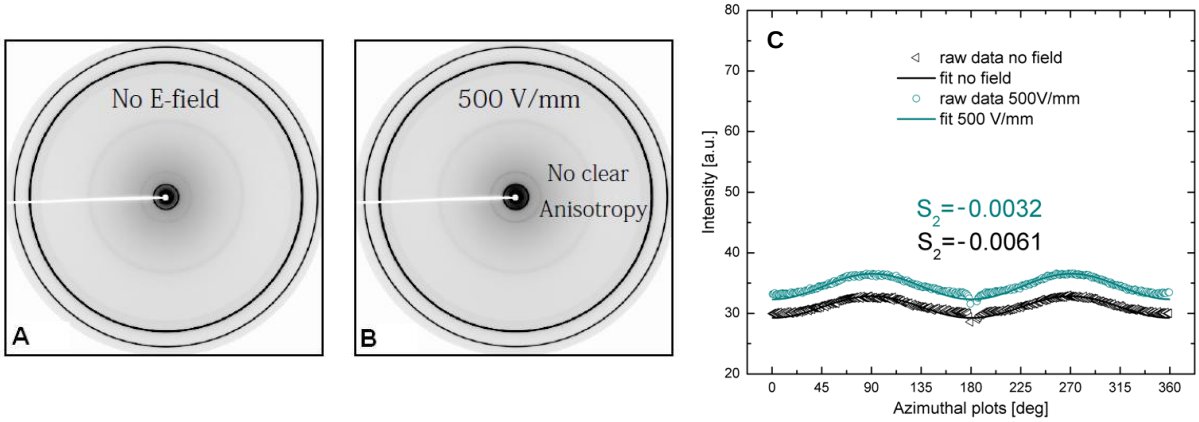

Fig. 8. WAXS 2-D images of Hal/paraffin composite without (A) and with (B) *E*-field of 500 V/mm. Azimuthal plots with calculated nematic order parameter (C).

Figure 9

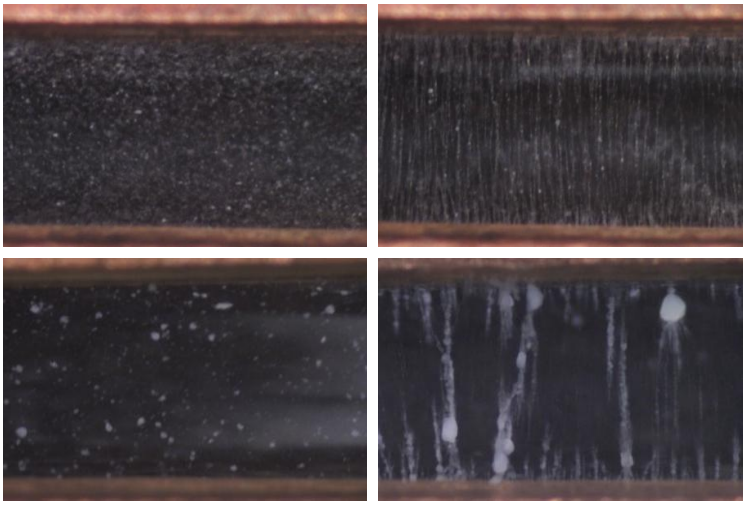

Fig. 9. Optical microscopy images of Kaol/silicone oil (top) and Hal/silicone oil (bottom) dispersions, without (left) and with *E*-field present (right). The gap between electrodes is 1 mm.

Figure 10

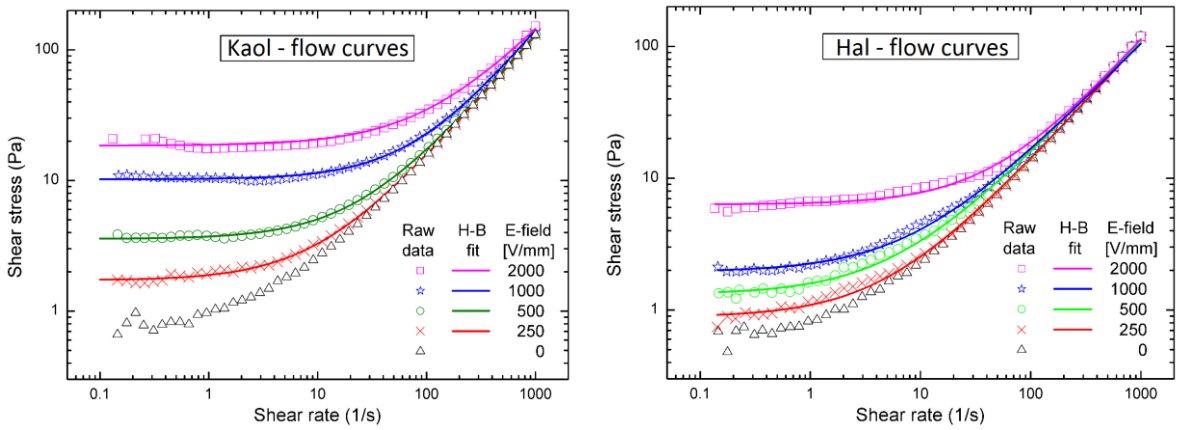

Fig. 10. Log-log plot of the flow curves of Kaol (left) and Hal (right) ER dispersions with particle concentration of Φ~5 m%. Experimental data are represented by symbols and the corresponding H-B fits are drawn using solid lines. (Measurements taken at 750 are not shown for sake of clarity, but the results are included in Table 1)

Figure 11

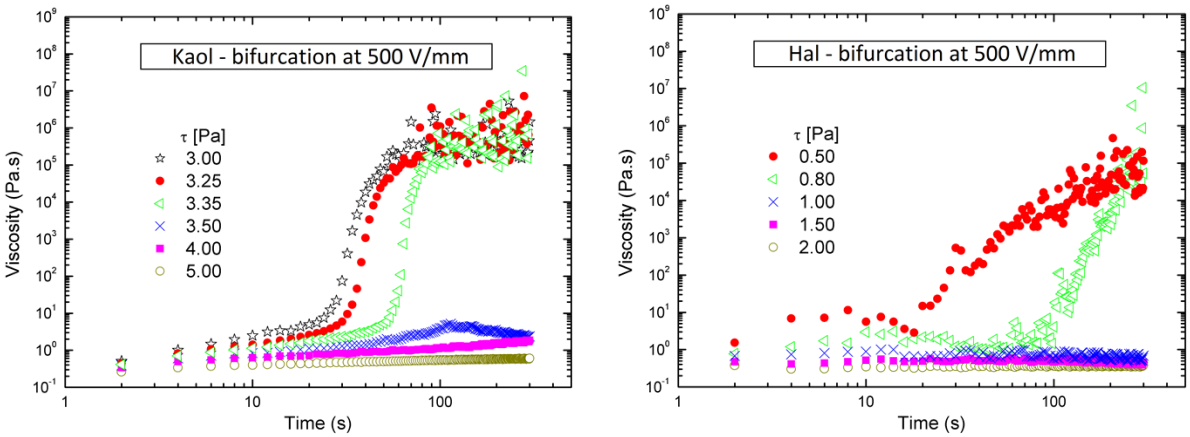

Fig. 11. Example of bifurcation in the rheology of Kaol (left) and Hal (right) dispersions in presence of *E*-field strength of 500 V/mm. Here the yield stresses are 3.3±0.1 and 0.9±0.1 Pa for Kaol and Hal, respectively.